VERIZONA PUBLISHER
Publishing Your Ideas

www.verizonaonlinepublishing.com
Vol: 1, Issue: 2

Journal of Nanoscience with Advanced Technology

Morphology, Microchemistry, Structural and Hydrogenation Characteristics of (Zr-Ti) $(Cr-V-Ni)_2$ Intermetallic Compounds

A. Ioannidou[1], S.S. Makridis[2], E. S. Kikkinides[2], A. K. Stubos[3], M. Gjoka[1], A. Prodan[4], E. Zupanič[4] and G. Kapun[5]

[1]Institute of Nanoscience and Nanotechnology, NCSR "Demokritos", Ag. Paraskevi, Athens, GR-15310, Greece
[2]Department of Mechanical Engineering, University of Western Macedonia, GR-50100, Kozani, Greece
[3]Institute of Nuclear & Radiological Sciences and Technology, Energy & Safety (INRASTES), NCSR "Demokritos", Ag. Paraskevi, Athens, GR-15310, Greece
[4]Department of Solid State Physics, Jožef Stefan Institute, Ljubljana, 1000, Slovenia
[5]National Institute of Chemistry, Ljubljana, 1000, Slovenia

***Corresponding author:** Dr. Alexandra Ioannidou, Institute of Nanoscience and Nanotechnology, NCSR "Demokritos", Ag. Paraskevi, Athens, GR-15310, Greece; Tel: +30 2130263410 ; Email : a.ioannidou@inn.demokritos.gr

Article Type: Research, **Submission Date**: 27 August 2015, **Accepted Date:** 16 September 2015, **Published Date:** 6 October 2015.

Citation: A Ioannidou , SS Makridis, ES Kikkinides, AK Stubos, M Gjoka, et al. (2015) Morphology, Microchemistry, Structural and Hydrogenation Characteristics of (Zr-Ti) $(Cr-V-Ni)_2$ Intermetallic Compounds. J Nanosci Adv Tech 1(2): 17-29. doi: https://doi.org/10.24218/jnat.2015.08.

Abstract

Hydrogen is a promising alternative fuel since it can be used pollution-free and can readily be produced from renewable energy resources, eliminating the production of greenhouse gases. Its storage is a great subject of intensive research for many years. Metal hydrides have the potential for reversible on-board hydrogen storage and release at low temperatures and pressures. In this work materials with nominal composition $Zr_{1-x}Ti_xCr_{2-y-z}V_yNi_z$ were investigated. The samples were prepared by arc-melting under Ar-atmosphere from pure metals. The structure and microstructure of the alloys were examined by X-ray diffraction analysis and high resolution scanning electron microscopy (HR-SEM), respectively. Morphology and quantitative measurement were made using the energy dispersive X-ray. A two phase system of hexagonal Laves $MgZn_2$ (C14)- and $MgCu_2$ (C15)-type of structure has been found for all samples. Increasing the V concentration in the stoichiometry leeds to development of a dentritic-type of microstructure. P-C-T curves were obtained after crucial activation procedure. The alloys were found to be more active under hydrogen while the desorbed amount of hydrogen has been measured in the temperature range of (20 to 30)°C by using a Sieverts'-type apparatus.

Keywords: Metal hydrides, Laves phases, Crystal structure, P-C-T curves

Introduction

Environmental problems related to the emission of greenhouse gases in conjunction with the depletion of fossil-fuel natural resources, have led to intensive research on alternative, environmentally friendly, fuels. The simultaneous growth of the world population and air-pollutant emissions produced by conventional fuels, impose their replacement by cleaner fuels such as hydrogen, which is well suited for electric-vehicle use [1-4].

Hydrogen is an attractive alternative fuel. However, unlike carbonaceous fuels, its role resembles more closely that of electricity as a secondary 'energy carrier', which must be first produced using energy from another source and then stored or transported for future use in the production of energy. The importance of hydrogen as a potential energy carrier has increased significantly over the last decade, owing to rapid advances in fuel cell technology, which produces electricity and water as a by-product.

The need for a worldwide conversion from fossil fuels to hydrogen requires the elimination of several barriers imposed along the different steps involved in hydrogen technology. Commercially viable hydrogen storage is considered as one of the most crucial and technically challenging barriers to the widespread use of hydrogen as an effective energy carrier in the automotive industry [4-6]. Unfortunately, up to day there are no hydrogen storage systems that can meet all of the basic requirements for the development of feasible hydrogen storage systems for mobile applications. Presently commercially viable hydrogen storage technologies have been focused around high-pressure gas vessels (250-700 bar) or liquefied hydrogen at cryogenic temperatures (20-30 K). One of the main advantages of compressed hydrogen gas storage is that it is a relatively simple and fast process since the filling of a vehicle tank can be completed in 3 min. The main disadvantages relate to the rather low volumetric and gravimetric densities at moderate pressure and temperature conditions in accordance with safety issues associated with extremely high-pressure hydrogen tanks that a common passenger car must carry during its operation. The main advantage of liquid hydrogen storage is that storage tanks can be filled in relatively short times and are much safer at appropriate cryogenic temperatures than high-pressure hydrogen tanks. The main disadvantages of liquid hydrogen storage are the high energy consumption associated with the liquefaction processes and continuous "boil-off" during storage [7]. The energy required to liquefy hydrogen is about

30-40% of the energy content of the gas and hence reduces significantly the overall efficiency of the system. An alternative to the above storage methods is proposed through the use of advanced solid materials as hosting agents for the storage of hydrogen in atomic or molecular form. This type of hydrogen storage is often called "solid" hydrogen storage since hydrogen becomes part of the solid material through some physicochemical bonding.

Metal hydrides have been seen as a potential means of hydrogen storage for over 35 years. The principle of hydrogen storage in metal hydrides is that atoms of hydrogen under low pressure bond chemically to the metal atoms. Since the process is exothermic hydrogen can be desorbed upon gentle heating. Many different alloy types exist, displaying a wide range of properties and performance characteristics, such as hydrogen content, desorption rate, cycle life and heat of reaction [8]. Metal hydrides compose of metal atoms that constitute a host lattice and hydrogen atoms. The major challenge in the development of efficient metal hydrides for hydrogen storage is to create a host lattice that satisfies three basic requirements: high volumetric and gravimetric hydrogen density, absorption-desorption reversibility and fast kinetics [9].

Metal hydrides are based on metallic alloys that absorb hydrogen gas, H_2. These alloys are combinations of group-A metals which can absorb H_2 independently (La, Ti, Zr Mg and Ca) with group-B metals which cannot absorb H_2 (Fe, Ni, Mn, Co and more) [10] and can be classified in the following categories:

a. Interstitial metal hydrides with a storage capacity of 1.8 wt% at 60–70 °C [11,12], or 3 wt% for quasi-crystalline Zr-Ti-Ni alloys [13,14] but with poor reversible hydrogen uptake.

b. Activated Mg-rich powders, reaching up to 5-6 wt% at 260-280 °C, where the kinetics needs to be improved.

c. Complex light–metal hydrides (alanates) which can absorb 5-8 wt% at slow rates.

Intermetallic compounds played an important role on developing hydrogen absorbing alloys. Sandia Hydrogen Information Center World Web site (http://hydpark.ca.sandia.gov) created a database which can be easily accessed electronically [15]. The class of intermetallics referred to as "Laves phases" was first discovered in the early 20's and 30's by Laves who reported the characteristic properties of this group while Friauf studied the crystallographic structures of the $MgCu_2$ and $MgZn_2$ [16,17]. In "Pearson's Handbook of Crystallographic Data for Intermetallic Phases" more than 1400 binary and ternary Laves phases have been reported [18].

Although, Laves phases were discovered so early, the interest in these materials started to grow in the last two decades because these materials have become candidates for several applications [19, 20]. The AB_2 type represents a large class of materials for hydrogen storage for applications at ambient temperature. This type consists of group-A metals (rare earth elements like La, Ti, Zr and Mg) and group-B metals (Fe, Ni, Mn, Cr and Co) [21].

Three different types of structures are generally observed: the $MgCu_2$ type of structure (Strukturbericht symbol C15) which is a face-centered cubic belonging to the Space Group Fd3m (O_h^7), the $MgZn_2$ type of structure (Strukturbericht symbol C14) an hexagonal type belonging to the Space Group $P6_3/mmc$ (D_{6H}^4) with 4 formula units per unit cell and final, the $MgNi_2$ type of structure (Strukturbericht symbol C36) which belongs also to hexagonal space group $P6_3/mmc$ (D_{6H}^4) [16]. The structures of the polytypes are shown in Figure 1.

Among the different types of metal hydrides, Zr-based AB_2 alloys are the frontier hydrogen storage alloys due to their satisfactory hydrogen storage capacity [22-25]. These materials can be easily

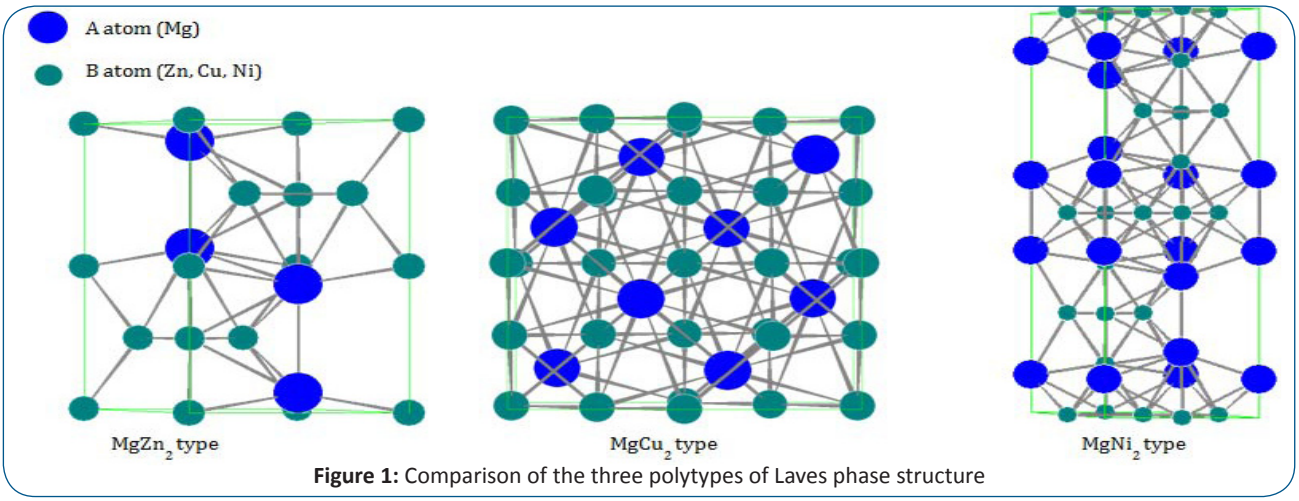

Figure 1: Comparison of the three polytypes of Laves phase structure

activated while they exhibit fast hydring-dehydring kinetics, good hydrogen capacity and can be used at atmospheric pressure and ambient temperature [26,27]. Although they seem to be promising materials they are not proposed for technological applications because of their high hydride stability [28].

One of the most useful methods to improve physical properties of hydrogen absorbing alloys is to perform substitutions on the A and B elements of the AB_2 Laves phase. Several studies have been made to explore and clarify the effect of replacing Zr with Ti in A site and elements such as V, Fe, Co, Ni, Mn and Al that occupy Cr on B site for the compound $ZrCr_2$.

Klein et al [29], Visintin et al [30] and Wu et al [31] observed that adding Ti to Zr site decreased hydrogen storage capacity while increased pressure plateau. Also, these authors have noted that a slope effect in the pressure plateau is due to the formation of the multi-component alloy and not the lack of annealing.

In the present work, the contemporary substitution of Ti in Zr

and V, Ni in Cr place in the $ZrCr_2$ alloy has been examined. Crystal structure characteristics of both alloys were determined by Rietveld analysis of the X-ray diffraction patterns, while micro-structural changes were examined by high resolution scanning electron microscopy (HR-SEM). Finally, the hydrogen storage capacity of the developed materials has been explored by applying a hydrogenation procedure on a Sievert-type apparatus at room temperature.

Experimental Procedure

The samples with nominal composition $Zr_{1-x}Ti_xCr_{2-y-z}V_yNi_z$ were prepared from pure metals (Zirconium 99.8%, Vanadium 99.7%, Titanium 99.9% Chromium 99% and Nickel 99,9%) using the method of arc-melting under argon atmosphere on a water-cooled crucible. To ensure homogeneity the samples with nominal composition $Zr_{1-x}Ti_xCr_{2-y-z}V_yNi_z$ (where x=0.1, 0.2 and 0.3, y=z=0.4 and 0.8) were turned over three times by turning them up and down with the help of the tungsten tip. The as-cast ingots were polished with glass paper to clean the surface from oxides and dirt and crushed into fine powder in a planetary mill (Retsch PM 400/2) with stainless steel balls under Ar-atmosphere.

X-ray diffraction analysis (Siefert 3003 TT, Siemens XD-500) using Cu-K_α (λ=1.54059 angstrom) radiation at 40 kV and 30 mA were used to study the crystal structure and the lattice parameters of the samples.

The microstructure of polished cross sections of the ingots was examined with a JSM 5800 SEM with an energy dispersive X-ray spectrometer (EDAX).

The samples were initially activated at 150°C in order to remove impurities and oxides and free interstitial sites for hydrogen to occupy. After one cycle of activation were measured at a temperature range of 25°C - 30°C and pressure of 40 bar. The pressure–composition isotherms (P–C curves) were measured using a Sieverts'–type apparatus in order to quantitatively characterize the hydrogen absorption and desorption behavior of the alloys. The purity of the hydrogen gas used for these measurements was better than 99.99%.

Polished sample surfaces were studied using ultra-high vacuum scanning tunneling micrsocope (UHV-STM) with base pressure 1 x 10^{-10} torr. The samples were cleaned in-situ by repeated cycles of ion bombardment (Ar^+ ions, 1 keV, 3 μA). STM imaging was done at room temperature in the constant-current mode.

Rietveld analysis was used to refine the X-ray diffraction patterns with the RIETICA program. This method uses a least squares fitting approach to adjust a theoretical line profile until it matches the experimentally measured profile. Since, the Rietveld method adjust, also the background it improves the treatment of weak diffraction peaks. Moreover, it takes care of the line overlapping problem [32].

Results and discussion

X-ray analysis showed that $ZrCr_2$ appeared with either of the two main Laves phases: C14 hexagonal phase with space group $P6_3/mmc$, which was the main phase of 97 % in the system and C15 cubic phase with space group Fd3m. Small peaks at lower angles which are not identified belong probably to the Zr. Figure 2 shows the X-ray diffraction patterns of non-hydrogenated alloys while in Table 1 the calculated patterns are shown after the fitting procedure, including the R-parameters and the structural parameters for all samples.

Substituting Zr with Ti and Cr with V led to the compound with

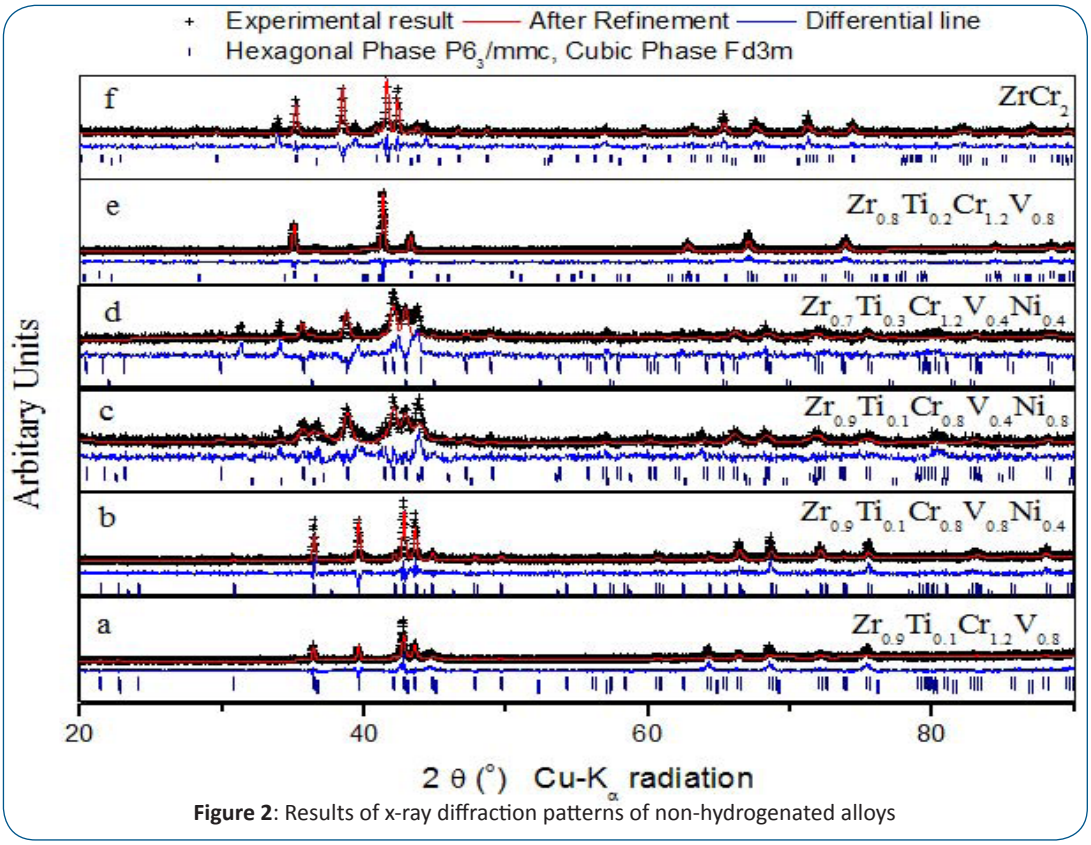

Figure 2: Results of x-ray diffraction patterns of non-hydrogenated alloys

Table 1: Phases, lattice parameters and parameters of the alloys after refinement

Alloy	Phase	Space Group	Lattice parameters [Å]		Derived R_{Bragg}	Wt%	χ^2	R_{wp}	R_{exp}
$ZrCr_2$	C14	$P6_3/mmc$	a=b=5.092	c=8.2702	9.58	97.42	1.673	24.02	18.57
	C15	Fd3m	a=b=c=6.9354		10.70	2.58			
$Zr_{0.9}Ti_{0.1}Cr_{1.2}V_{0.8}$	C14	$P6_3/mmc$	a=b=5.12	c=8.3309	15.84	51.48	0.378	13.91	22.62
	C15	Fd3m	a=b=c=6.9354		5.79	48.52			
$Zr_{0.9}Ti_{0.1}Cr_{0.8}V_{0.8}Ni_{0.4}$	C14	$P6_3/mmc$	a=b=5.1121	c=8.3302	11.48	88.25	0.831	19.53	21.43
	C15	Fd3m	a=b=c=7.000		5.57	12.75			
$Zr_{0.9}Ti_{0.1}Cr_{0.8}V_{0.4}Ni_{0.8}$	C14	$P6_3/mmc$	a=b=5.0461	c=8.2384	4.46	66.45	1.498	23.50	19.20
	C15	Fd3m	a=b=c=6.8665		12.57	28.93			
	C14	$P6_3/mmc$	a=b=3.2305	c=5.2619	9.72	4.62			
$Zr_{0.8}Ti_{0.2}Cr_{1.2}V_{0.8}$	C14	$P6_3/mmc$	a=b=5.23	c=8.8055	5.52	24.25	0.467	16.59	24.27
	C15	Fd3m	a=b=c=7.2573		12.46	75.75			
$Zr_{0.7}Ti_{0.3}Cr_{1.2}V_{0.4}Ni_{0.4}$	C14	$P6_3/mmc$	a=b=5.0342	c=8.2382	17.77	92.76	2.374	20.39	13.23
	C15	Fd3m	a=b=c=6.9965		8.65	7.24			

nominal composition $Zr_{0.9}Ti_{0.1}Cr_{1.2}V_{0.8}$. Adding V into Cr sites decreases the fraction of the hexagonal phase and increases the cubic one to almost 50 wt% with a small derived R_{Bragg}.

As a next step we studied the effect of Ni at the B site. The compounds formed with this substitution belong to the general stoichiometry $Zr_{1-x}Ti_xCr_{2-y-z}V_yNi_z$. For x=0.1, y=0.8 and z=0.4 the Rietveld analysis showed two phases, a main phase identified as $ZrCr_2$ with C14 structure and a second one with the C15 structure with a smaller weight percentage. Figure 3 shows a detailed diffraction pattern after fitting. Small grey rhombohedra indicate the peaks belonging to the cubic phase. All the other peaks belong to the hexagonal phase.

In case of reduced V and increased Ni content, e.g. $Zr_{0.9}Ti_{0.1}Cr_{0.8}V_{0.4}Ni_{0.8}$ the grain structure consists of smaller grains and the corresponding peaks in the x-ray diffraction spectra appear considerably wider.

A partial replacement of Zr by Ti in $ZrCr_2$ with the simultaneous substitution of Cr by V and Ni increased the lattice parameters of the cell and led to the conversion of the hexagonal phase C14 ($P6_3/mmc$) into the cubic Laves phase C15 (Fd3m). Thus, the cubic phase became the main phase and hexagonal one the second with 25 wt% only. Small amounts of further phases remain to be identified.

The last sample examined by x-ray analysis had the composition $Zr_{0.7}Ti_{0.3}Cr_{1.2}V_{0.4}Ni_{0.4}$. Additional peaks detected at lower angles belong to an unidentified Zr-rich phase. In Figure 4 Rietveld analysis of the hydrogenated alloys is shown. In comparison with as-cast samples, no new peaks were detected and the existing

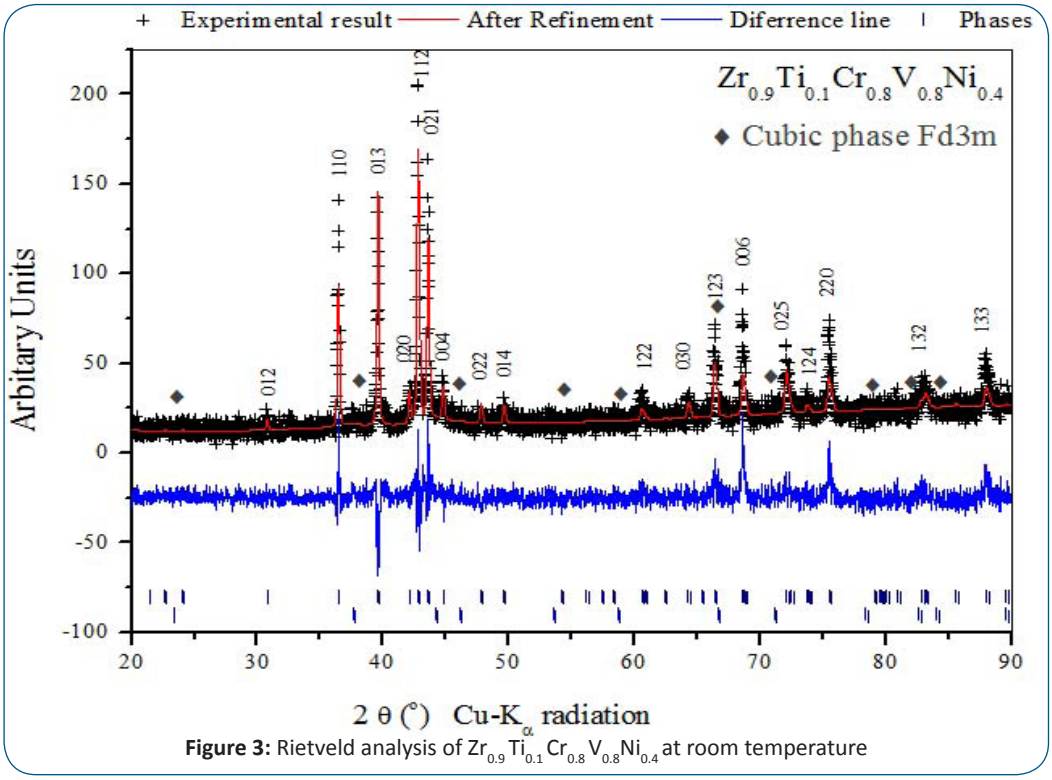

Figure 3: Rietveld analysis of $Zr_{0.9}Ti_{0.1}Cr_{0.8}V_{0.8}Ni_{0.4}$ at room temperature

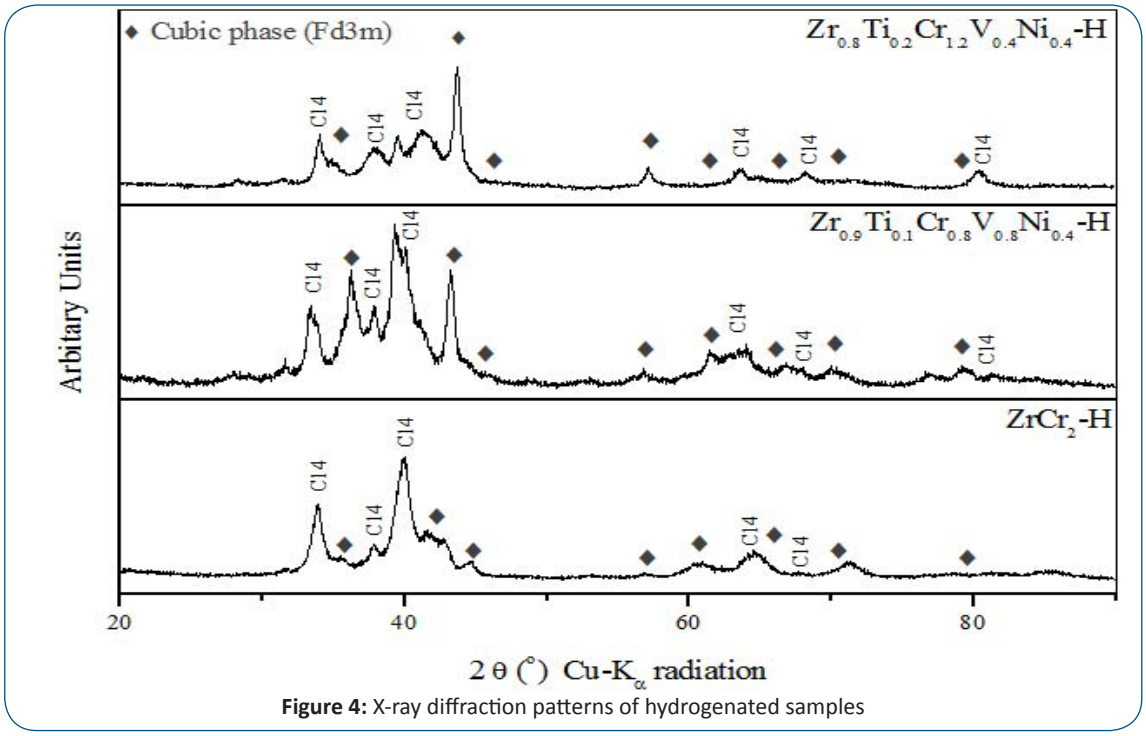

Figure 4: X-ray diffraction patterns of hydrogenated samples

ones were shifted toward lower angles. This is in agreement with the increased amount of H and the decreased average grain sizes after cycles of hydrogenation-dehydrogenation. The results of X-ray patterns after the fitting procedure, including the R-parameters and the structural parameters for all samples are shown in Table 2.

Theoretical investigation was also performed for x-ray diffraction patterns in order to understand the diffusivity effect of the substitutions on the intensities of the (hkl) planes. Figure 5 shows these calculations where the analysis suggests that (Cr, V, Ni) atoms occupy also A-site.

In order to study into more detail the microstructure of the materials HR-SEM studies were performed. The results of these studies are shown in Figure 6 and Figure 7. All samples show a

Table 2: Phases, lattice parameters and parameters of the hydrogenated alloys after refinement

Alloy	Phase	Space Group	Lattice parameters [Å]		Derived R_{Bragg}	Wt%	χ^2	R_{wp}	R_{exp}
$ZrCr_2$	C14	$P6_3/mmc$	a=b=5.092	c=8.2702	9.58	97.42	1.673	24.02	18.57
	C15	Fd3m	a=b=c=6.9354		10.70	2.58			
$Zr_{0.9}Ti_{0.1}Cr_{0.8}V_{0.8}Ni_{0.4}$	C14	$P6_3/mmc$	a=b=5.3581	c=8.7825	14.59	86.91	18.841	31.76	7. 32
	C15	Fd3m	a=b=c=6.9216		28.41	13.09			
$Zr_{0.8}Ti_{0.2}Cr_{1.2}V_{0.4}Ni_{0.4}$	C14	$P6_3/mmc$	a=b=5.0342	c=8.2382	17.77	92.76	2.374	20.39	13.23
	C15	Fd3m	a=b=c=6.9965		8.65	7.24			

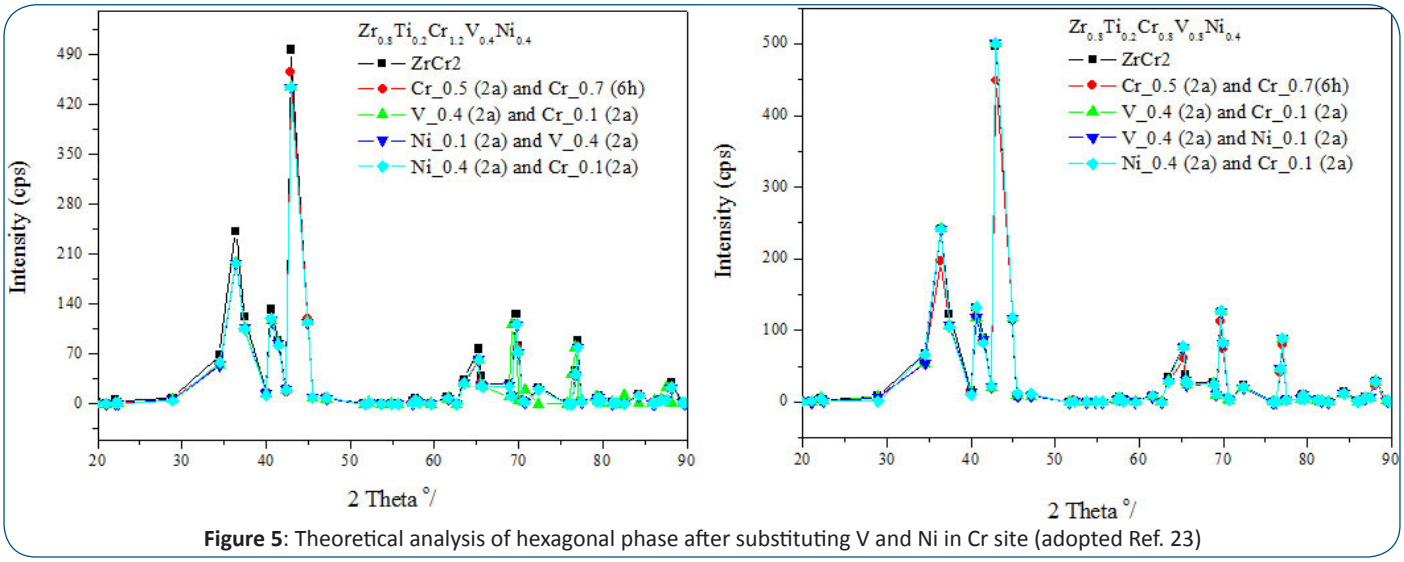

Figure 5: Theoretical analysis of hexagonal phase after substituting V and Ni in Cr site (adopted Ref. 23)

multiphase structure with the hexagonal phase C14 contributing the grey areas in all samples examined. This is clearly confirmed by the EDAX analyses shown in Table 3. A more uniform morphology was detected only in case of $Zr_{0.9}Ti_{0.1}Cr_{0.8}V_{0.8}Ni_{0.4}$ (Figure 6b). Further analysis showed that this composition is a two phase system with the same percentage of each phase. Thus

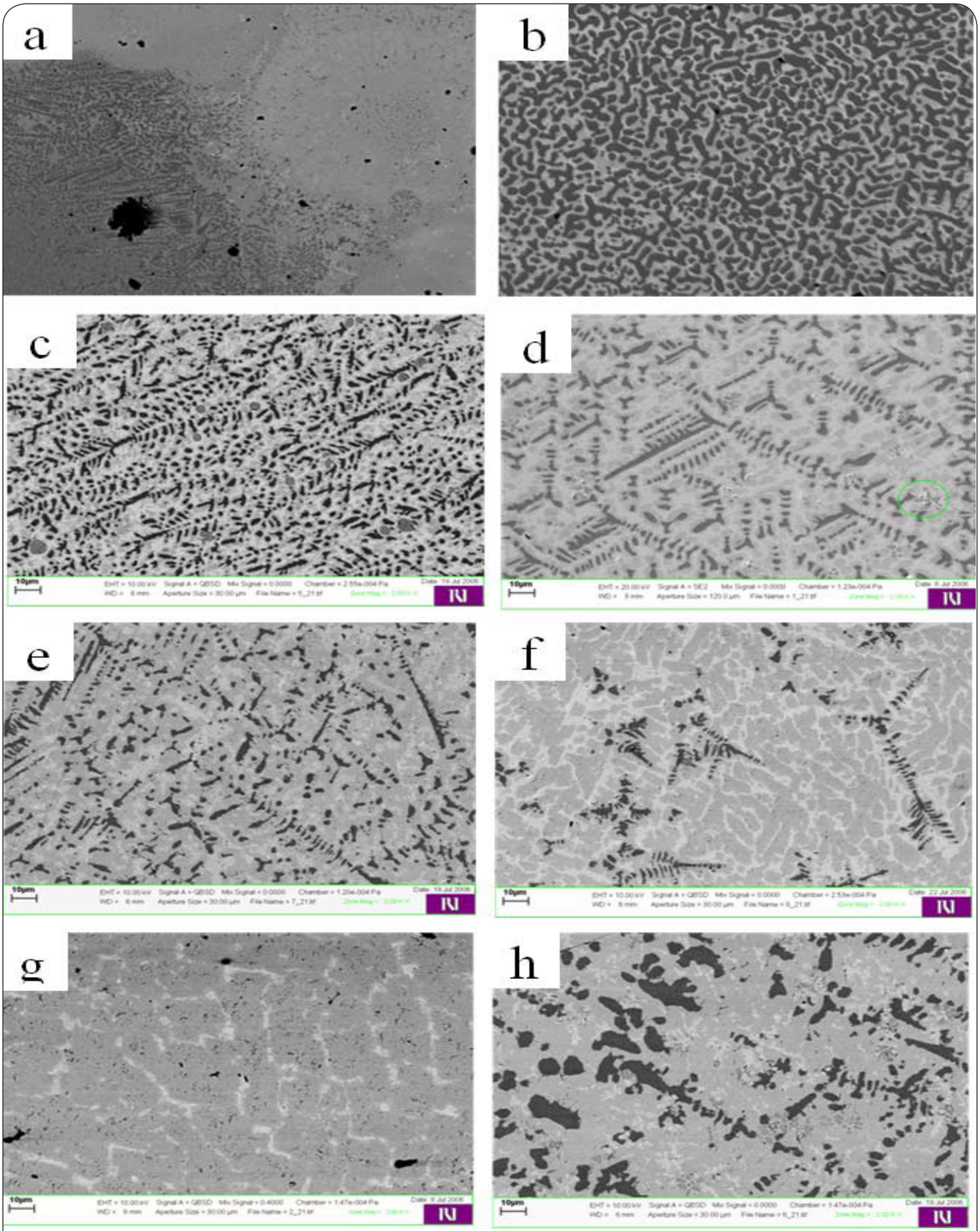

Figure 6: SEM analysis of samples: a) $Zr_{0.9}Ti_{0.1}Cr_{1.2}V_{0.8}$ b) $Zr_{0.9}Ti_{0.1}Cr_{0.8}V_{0.8}Ni_{0.4}$ c) $Zr_{0.9}Ti_{0.1}Cr_{0.4}V_{0.8}Ni_{0.8}$, d) $Zr_{0.9}Ti_{0.1}Cr_{0.8}V_{0.4}Ni_{0.8}$, e) $Zr_{0.8}Ti_{0.2}Cr_{0.8}V_{0.8}Ni_{0.4}$ f) $Zr_{0.8}Ti_{0.2}Cr_{0.8}V_{0.4}Ni_{0.8}$ g) $Zr_{0.8}Ti_{0.2}Cr_{1.2}V_{0.4}Ni_{0.4}$, and h) $Zr_{0.7}Ti_{0.3}Cr_{1.2}V_{0.4}Ni_{0.4}$

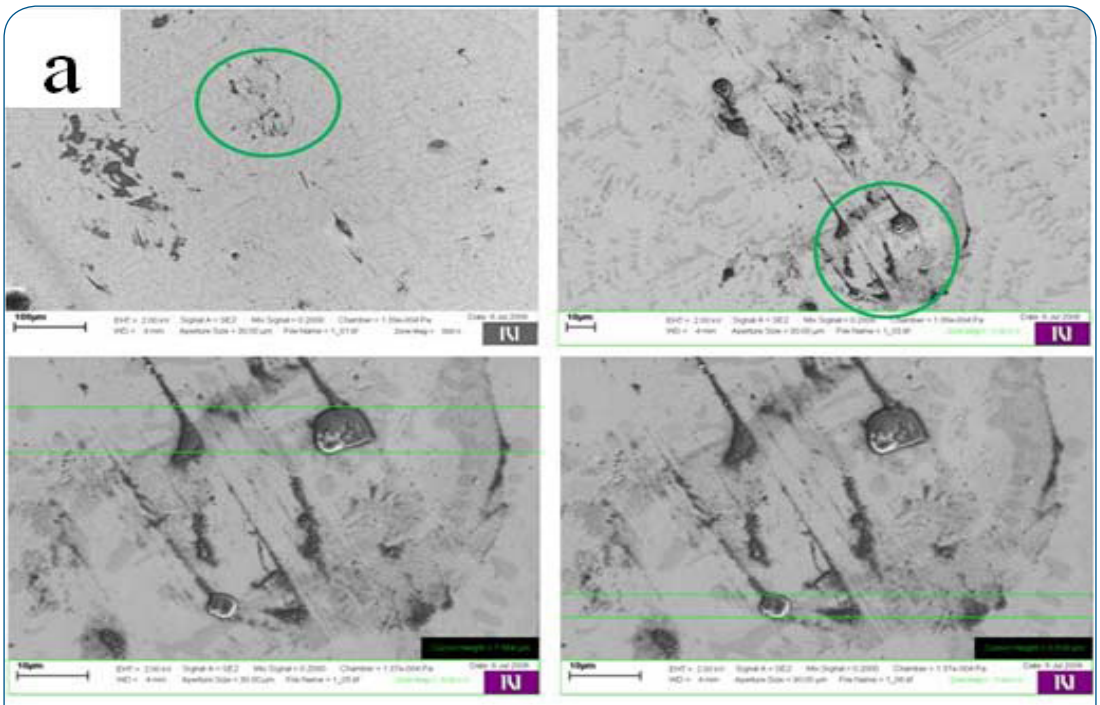

Figure 7a: Analysis of agglomerates and defects on microstructure of the sample $Zr_{0.9}Ti_{0.1}Cr_{0.8}V_{0.4}Ni_{0.8}$

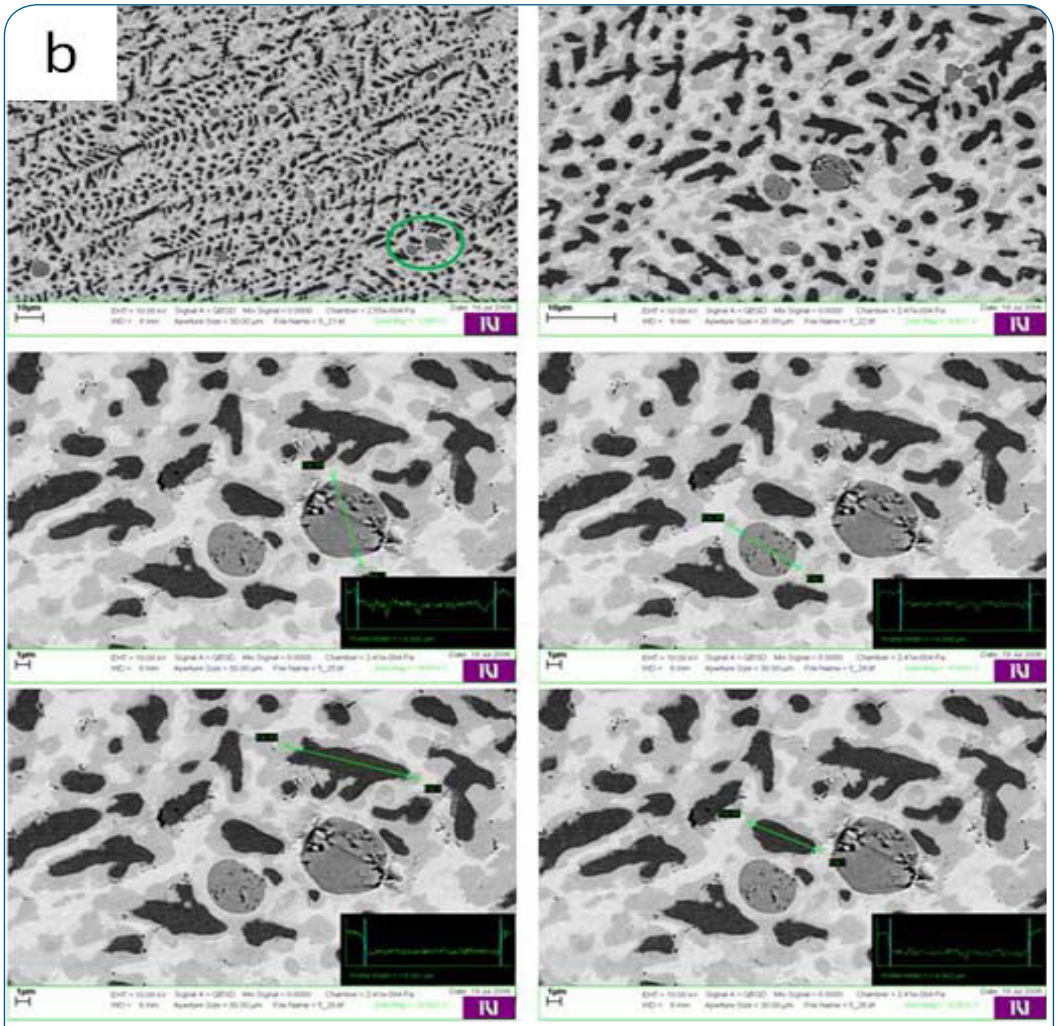

Figure 7b: Analysis of agglomerates and defects on microstructure of the sample $Zr_{0.9}Ti_{0.1}Cr_{0.4}V_{0.8}Ni_{0.8}$

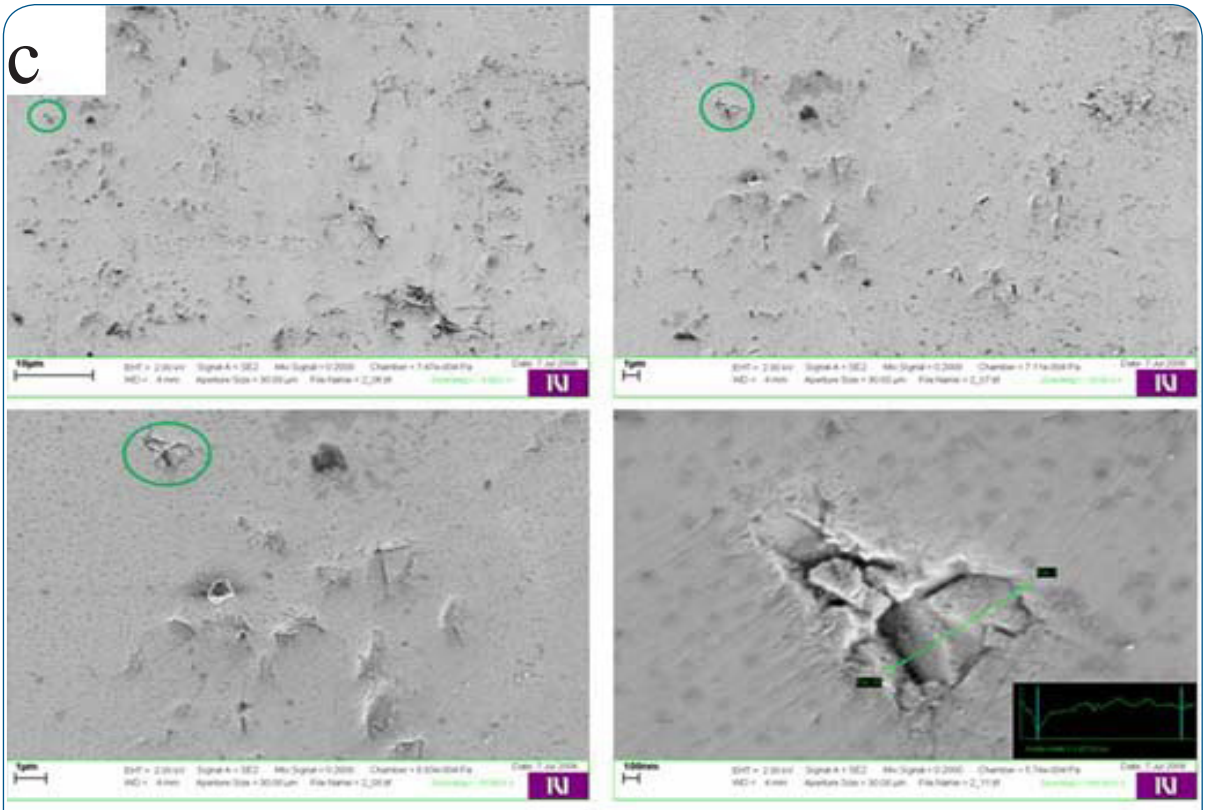

Figure 7c: Analysis of agglomerates and defects on microstructure of the sample $Zr_{0.8}Ti_{0.2}Cr_{1.2}V_{0.4}Ni_{0.4}$

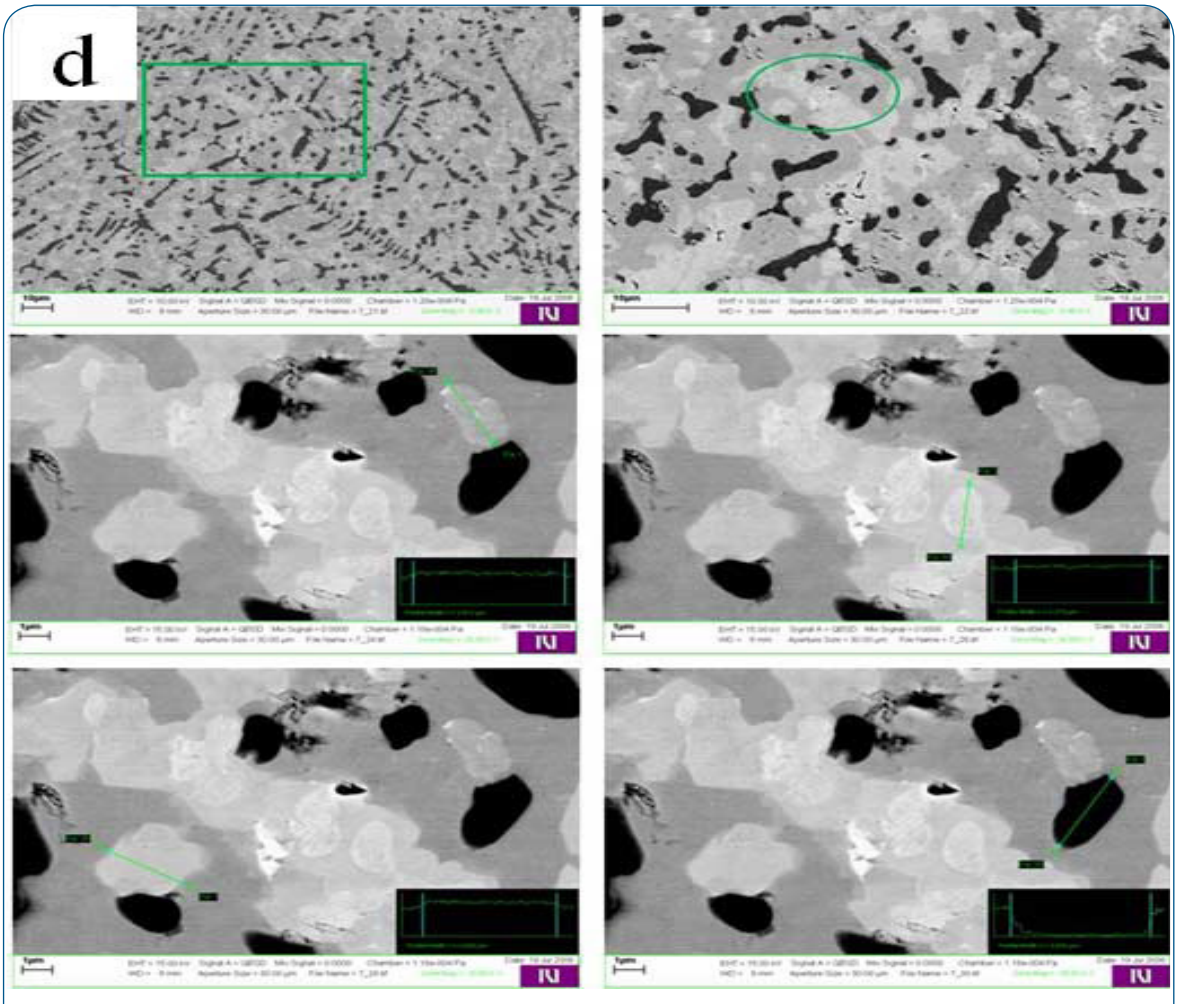

Figure 7d: Analysis of agglomerates and defects on microstructure of the sample $Zr_{0.8}Ti_{0.2}Cr_{0.8}V_{0.8}Ni_{0.4}$

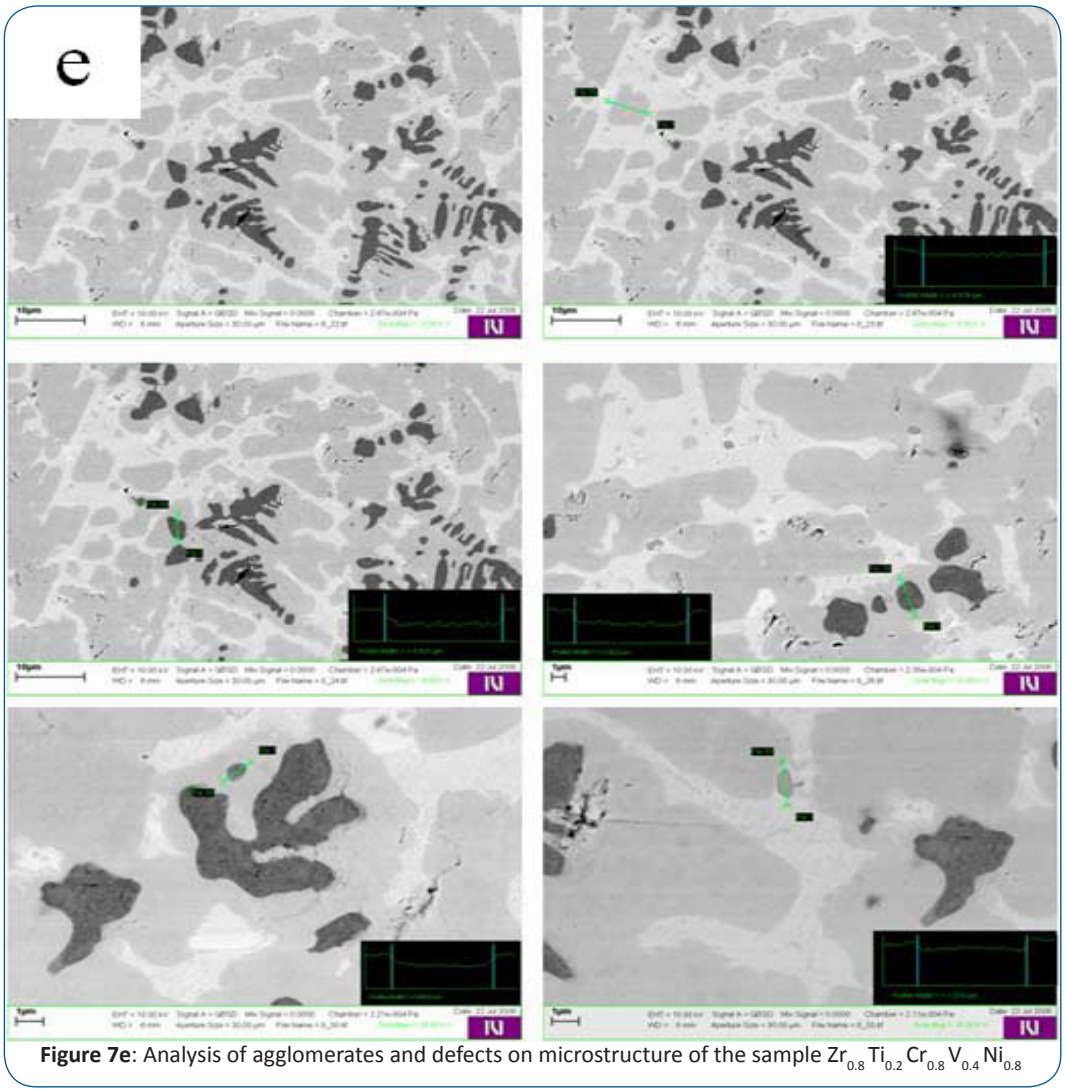

Figure 7e: Analysis of agglomerates and defects on microstructure of the sample $Zr_{0.8}Ti_{0.2}Cr_{0.8}V_{0.4}Ni_{0.8}$

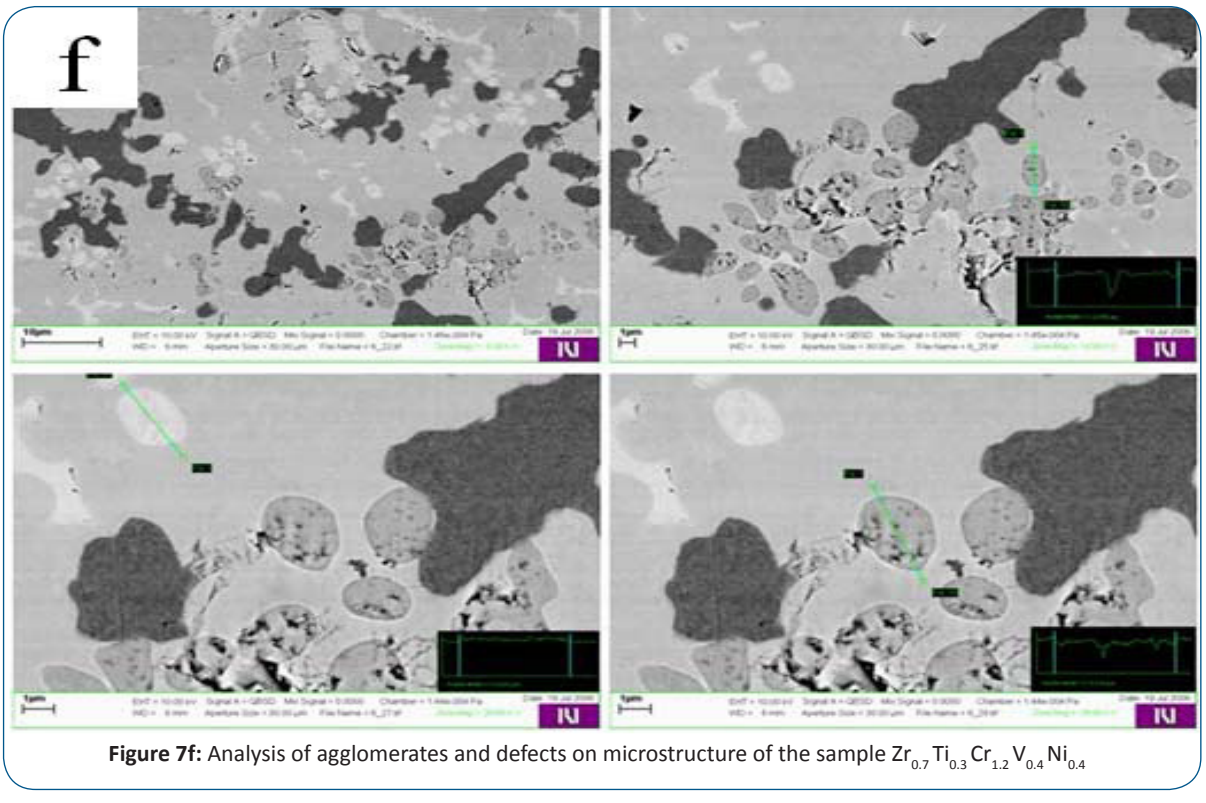

Figure 7f: Analysis of agglomerates and defects on microstructure of the sample $Zr_{0.7}Ti_{0.3}Cr_{1.2}V_{0.4}Ni_{0.4}$

Table 3: HR-SEM analysis of all samples

Alloy	Area	Metal	Zr	Ti	Cr	V	Ni	O
$Zr_{0.9}Ti_{0.1}Cr_{1.2}V_{0.8}$	White	Not present						
	Black		56.03	1.60	31.96	10.41	------	------
	Grey (matrix)		47.15	7.91	27.73	17.21	-------	-------
	Dark Grey (Zr)	Not present						
$Zr_{0.9}Ti_{0.1}Cr_{0.8}V_{0.8}Ni_{0.4}$	White	Not present						
	Black (Cr-V)		3.57	17.94	7.20	71.28	-------	-------
	Grey (matrix)		57.79	21.68	2.21	17.99	0.34	------
	Dark Grey (Zr)	Not present						
$Zr_{0.9}Ti_{0.1}Cr_{0.4}V_{0.8}Ni_{0.8}$	White		58.68	------	0.53	0.79	36.93	------
	Black (Cr-V)		3.94	------	32.28	58.39	4.45	------
	Grey (matrix)		21.90	0.24	20.62	39.36	16.21	------
	Dark Grey (Zr)		70.52	----	0.29	0.27	0.83	26.14
$Zr_{0.9}Ti_{0.1}Cr_{0.8}V_{0.4}Ni_{0.8}$	White		53.95	3.29	1.30	0.82	37.58	------
	Black (Cr-V)		0.82	0.95	63.81	32.68	1.74	------
	Grey (matrix)		41.98	2.07	25.74	9.13	19.07	------
	Dark Grey (Zr)		94.38	------	1.14	0.71	2.70	------

Alloy	Area	Metal	Zr	Ti	Cr	V	Ni
$Zr_{0.8}Ti_{0.2}Cr_{0.8}V_{0.8}Ni_{0.4}$	White		59.69	6.24	2.07	3.01	25.04
	Black (Cr-V)		2.90	2.63	41.27	50.15	1.61
	Grey (matrix)		57.15	4.31	11.76	12.75	10.45
	Dark Grey (Zr)		83.48	2.24	1.25	1.43	1.38
$Zr_{0.8}Ti_{0.2}Cr_{0.8}V_{0.4}Ni_{0.8}$	White		46.99	8.55	0.77	1.06	38.89
	Black (Cr-V)		1.85	1.69	56.47	36.11	2.21
	Grey (matrix)		39.52	3.67	24.93	10.75	18.00
	Dark Grey (Zr)	Not present					
$Zr_{0.8}Ti_{0.2}Cr_{1.2}V_{0.4}Ni_{0.4}$	White		55.00	4.63	1.22	0.79	33.84
	Black (Cr-V)	Not present					
	Grey (matrix)		39.67	4.63	30.30	11.48	11.09
	Dark Grey (Zr)		91.49	0.85	1.20	0.81	1.56
$Zr_{0.7}Ti_{0.3}Cr_{1.2}V_{0.4}Ni_{0.4}$	White	Not present					
	Black (Cr-V)		----	2.37	68.86	26.99	1.03
	Grey (matrix)		37.42	5.83	29.70	9.09	15.56
	Dark Grey (Zr)		91.41	3.59	0.57	0.36	0.92

the sample is composed two hexagonal phases with different microchemistry. The first of these two phase represent V-poor areas which appear light in the SEM images, while the second belongs to V-rich areas and appears black. Rietveld analysis show that both belongs to the AB_2 hexagonal phases with symmetry $P6_3/mmc$. Almost 88 wt% belongs to the AB_2 composition with A=Zr, Ti and B=Cr, Ni, while in the second phase Ni is replaced by V. If the amount of V is increased on account of Cr, a dendritic microstructure is developed (Figure 6c). Black area, belong to the V-rich phase. Grey dots on the surface of this sample were analyzed by EDAX as Zr which represents the third phase in this alloy. On the contrary, Figure 6d shows the effect of decreasing V while increasing Ni atom. The dendritic type of structure is still evident, but there are some non-homogeneous areas relates to the procedure of activation/hydrogenation/dehydrogenation. Figure 6e to 6h show the dependence of the microstructure as a function of Ti substitution for Zr in A-sites. The microstructure seems to change morphology and the dendrites are disappearing. The morphology is more composite and can be seen from the changes in brightness which is associated with changes in chemistry. In

Figure 6g where the Cr percentage (60 at%) increased, a non-dendritic microstructure appeared.

Furthermore, chemical mapping was performed in order to understand better the atomic diffusivity of the samples. Figure 8a-f show two main phases revealed in the microstructure, i.e. the V–Cr and the Zr–Ti–Ni, as revealed by the x-ray analysis. Vanadium and chromium areas appear as the black region while, titanium and nickel appear grey. Zr is distributed also in grey areas as small inclusions [33]. It is noted that defects appearing in the microstructure of the samples are more apparent even after the chemical treatment. The emergence of different microchemistry between dendrites and regional provision continues to exist for all samples. Micro-dendrites form a microchemistry that drastically affects to the hydrogenation properties and the kinetics.

In addition to SEM, STM was also performed on the sample $Zr_{0.9}Ti_{0.1}Cr_{0.8}V_{0.8}Ni_{0.4}$ (Figure 9). Figure 9a was recorded after initial ion-etching and it shows small round shaped agglomerates with average diameter below 5 nm. Figure 9b was recorded after additional annealing was performed and it shows round shaped partly ordered agglomerates with a boundary between two larger domains. These boundaries correspond to the domain boundaries observed in most SEM images.

Pressure–composition results are shown in Figure 10. The measurement obtained at temperature range of 25–30˚C after activation procedure at 150˚C. Before this procedure the capsule with the sample remained in vacuum overnight in order to clean the surface from "dirt". $ZrCr_2$ is a very stable compound [29-30, 34] and cannot absorb a large quantity of hydrogen. After substituting Zr with Ti and Cr with V, Ni hydrogen capacity increased while hysteresis decreased. $Zr_xTi_{1-x}Cr_{0.8}V_{0.8}Ni_{0.4}$ for x=0.1 and 0.2 showed the highest hydrogen capacity at 30˚C, 2.42 H/M (~1.25 wt%) and 2.16 H/M (~1.16 wt%), respectively. Comparing these two compounds revealed that adding Ti content in Zr site the hydrogen capacity decreased while pressure plateau increased. This comes to a good agreement with literature where previous works showed that small superinduction of Ti decreases the stability of the hydride at room temperature [30, 35]. An interesting conclusion came also from these hydrogenations concerns the alloys in Figure 10e and Figure 10f with a nominal composition of $Zr_{0.8}Ti_{0.2}Cr_{1.2}V_{0.4}Ni_{0.4}$ and $Zr_{0.8}Ti_{0.2}Cr_{0.8}V_{0.8}Ni_{0.4}$, respectively. As it can be seen from the results the effect of V improves the hydrogen capacity and the hysteresis problem. An interesting measurement of desorption shown in Figure 11 was carried out for the $Zr_{0.9}Ti_{0.1}Cr_{0.8}V_{0.8}Ni_{0.4}$. The experiment started at 25˚C where the desorbed quantity was ~200 ml/g (~1.7 wt%) in the first 10 min while at 97˚C after 15 min the overall desorbed hydrogen was found to be ~280 ml/g (~2.5 wt%) [36].

Using gravimetric method the alloy $Zr_{0.9}Ti_{0.1}Cr_{0.8}V_{0.8}Ni_{0.4}$ was analysed. Initially the material was activated at 250˚C and after 3 cycles was measured at 30˚C. The total amount of absorbed hydrogen was 4 wt% while the reversible capacity was only 1.5 wt%. It appears that in the material a hydrogen rate of about 2.3 wt% remains constant, which can be desorbed with increasing temperature. In first 10 hours the sample temperature changed at constant pressure in order to obtain activated granules. The absorption of hydrogen is reduced when the temperature and with increasing pressure. After 13.5 hours the temperature is constant at 30˚C we find that the change in pressure from 0 to 2,5 MPa and vice versa, or 0.1 MPa shows trends change in storage capacity with continuous increase in the maximum absorption rate at 2.5 MPa. This behavior is associated with the continuous activation of the granular material in the process of measurement and the approach of the 4% by weight of hydrogen in the league, despite the residual amount to 0 MPa is associated with the second phase AB_2 analyzed the microstructure and has different properties of the phase absorbs reversibly at 30˚C in 1.5%.

Conclusions

In the present work we studied Zr-based alloys of the type $Zr_{1-x}Ti_xCr_{2-y-z}V_yNi_z$. By means of x-ray Rietveld analysis we determined the phases existing in the samples. A system of two Laves phases was detected were C14 hexagonal was the main phase and C15 cubic phase being the second. The parallel substitution of Ti in Zr site and V and Ni in Cr position leaded to a change of the

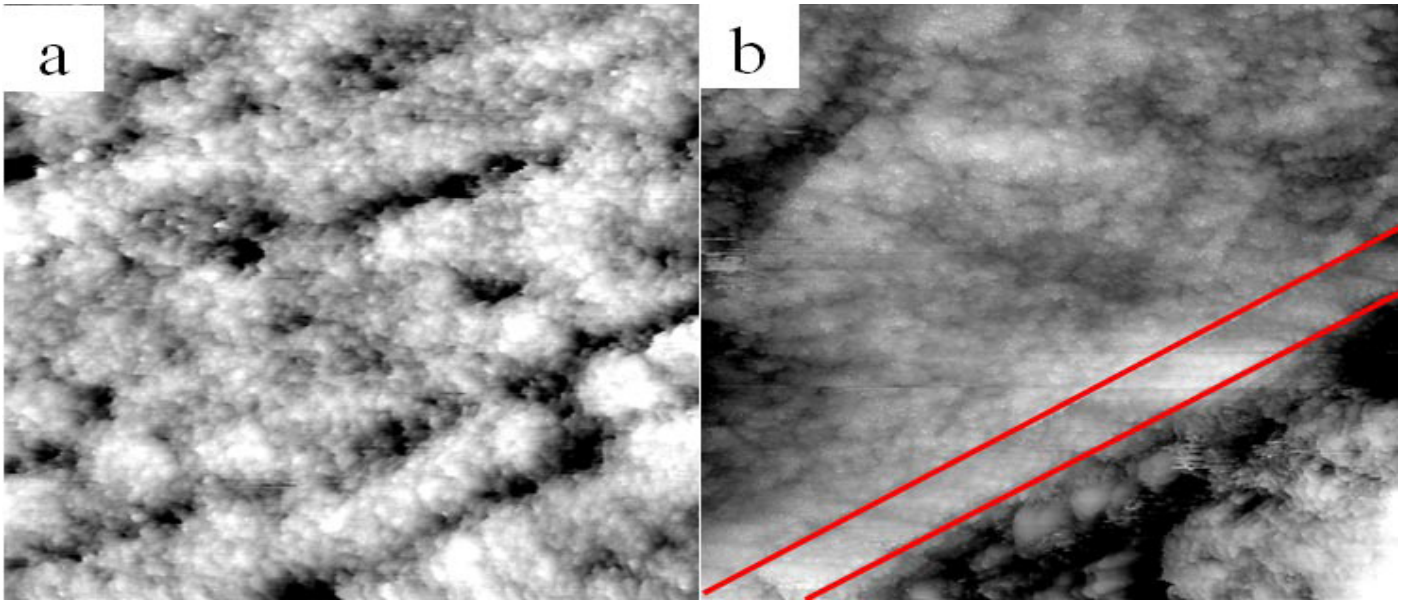

Figure 9: STM images of the alloy $Zr_{0.9}Ti_1Cr_{0.8}V_{0.8}Ni_{0.4}$ (sample b) a) After initial ion-etching[200 nm x 200 nm, ccm,Ug= 0.92 V, I_t= 0.63 nA], b) After additional annealing [200 nm x 200 nm, ccm, U_g = -0.83 V, I_t = 1. 06 nA]

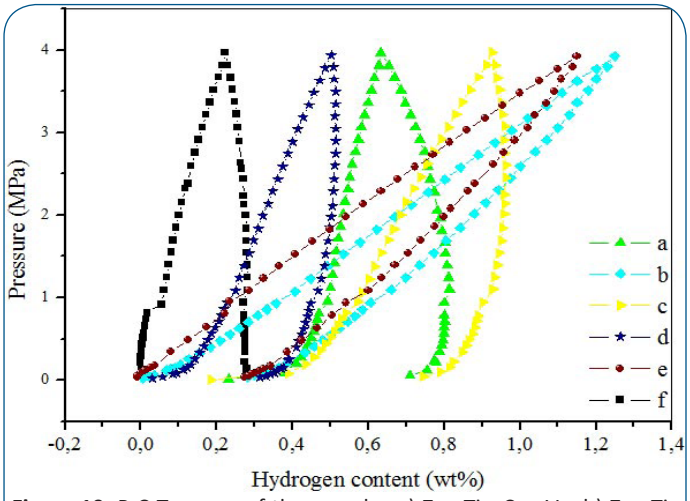

Figure 10: P-C-T curves of the samples a) $Zr_{0.9}Ti_{0.1}Cr_{1.2}V_{0.8}$ b) $Zr_{0.9}Ti_{0.1}Cr_{0.8}V_{0.8}Ni_{0.4}$, c)$Zr_{0.9}Ti_{0.1}Cr_{0.8}V_{0.4}Ni_{0.8}$, d) $Zr_{0.8}Ti_{0.2}Cr_{1.2}V_{0.4}Ni_{0.4}$, e) $Zr_{0.8}Ti_{0.2}Cr_{0.8}V_{0.8}Ni_{0.4}$ and f)$ZrCr_2$ at 25 and 30°C

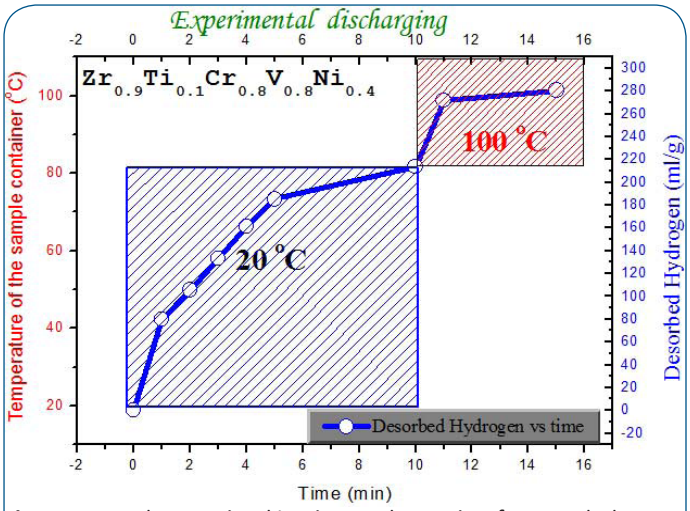

Figure 11: Hydrogenation kinetics on desorption for sample b, $Zr_{0.9}Ti_{0.1}Cr_{0.8}V_{0.8}Ni_{0.4}$ (adopted Ref. 29)

percentage of phases. Additionally, chemical mapping and EDAX analysis were also performed on SEM images, where a dendritic type of microstructure appeared in almost all samples.

The measured absorption – desorption isotherms showed the influence of the microstructure of the samples. The simultaneous substitution of A and B site of the main compound $ZrCr_2$ resulted to an increase in hydrogen capacity a decrease of pressure plateau. The samples initial were activated in the 150°C in order to remove impurities and oxides and release the interstitial sites occupied by hydrogen. Pressure/composition curves were measured in room temperature using volumetric method. The samples with the larger amount of hydrogen capacity where the ones with stoichiometry $Zr_{0.9}Ti_{0.1}Cr_{0.8}V_{0.8}Ni_{0.4}$ and $Zr_{0.8}Ti_{0.2}Cr_{0.8}V_{0.8}Ni_{0.4}$, resulted 1.25 wt% and 1.16 wt%, respectively. Due to the particular morphology and high storage capacity, the compound with stoichiometry $Zr_{0.9}Ti_{0.1}Cr_{0.8}V_{0.8}Ni_{0.4}$ was further more studied with the method of Scanning Tunelling Microscopy (STM) and the gravimetric method. The results of microscope analysis showed the existence of round agglomerates with diameter 5 nm and the existence of boundaries between two big domains. The pressure/composition measurement with the gravimetric method showed that at room temperature can be achieved high absorption capacity of 4 wt% while can desorb reversibly almost 2.3 wt%.

Acknowledgments

This work was supported in part by the BILATERAL S & T Cooperation between the Hellenic Republic and the Republic of Slovenia (2004 – 2006), by the NESSHY European Program (Contract number: SES6-518271) and by the European Marie Curie ToK project DIAMANTE (C.N.: MTKI-CT-2005-0259544).

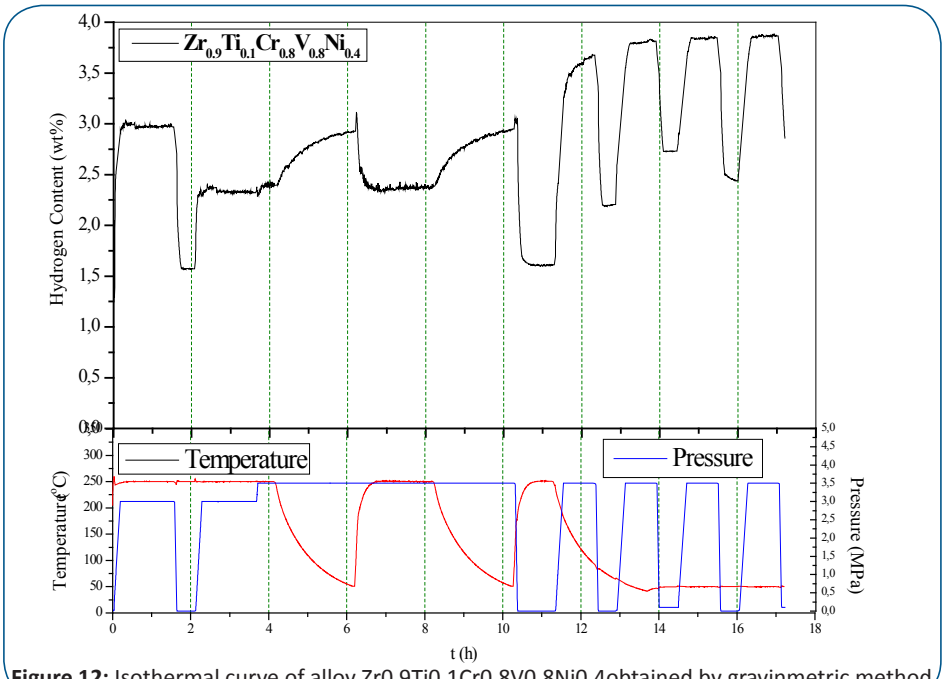

Figure 12: Isothermal curve of alloy Zr0.9Ti0.1Cr0.8V0.8Ni0.4obtained by gravinmetric method

References

1. Mohanty K. The near-term energy challenge.AICheJ. 2003; 49(10):2454–2460.doi: 10.1002/aic.690491002.
2. Momirlan M, Veziroglu TN. Current status of hydrogen energy. Renew. Sustain. Energy Rev. 2002; 6(1-2):141–179.doi:10.1016/S1364-0321(02)00004-7.
3. Agrawal R, Offutt MP, Michael P. Ramage. Hydrogen economy – an opportunity for chemical engineers.AICheJ. 2005; 51(6):1582–1589.doi: 10.1002/aic.10561.
4. Edwards PP, Kuznetsov VL, David WIF. Hydrogen energy. Phil. Trans. R. Soc. 2007; 365:1043–1056. doi:10.1098/rsta.2006.1965.
5. Crabtree GW, Dresselhaus MS, Buchanan MV. The hydrogen economy. Phys. Today. 2004; 57(12):39–44. doi: http://dx.doi.org/10.1063/1.1878333.
6. Harris R, Book D, Anderson PA, Edwards PP. Hydrogen storage: The grand challenge. Fuel Cell Rev. 2004; 1:17–23.
7. Zhang J, Fisher TS, Ramachandran PV, Gore JG, Mudawar I. A review of heat transfer issues in hydrogen storage technologies. J. Heat Transf. 2005; 127:1391–1399.
8. Sakintun B, LamariDarkrim F, Hirscher M. Metal hydride materials for solid hydrogen storage. A review, Int. J. Hydrog. Energy. 2007; 32(9):1121–1140. doi:10.1016/j.ijhydene.2006.11.022.
9. Crabtree GW, Dresselhaus MS. MRS Bulletin. 2008; 33:421–428.
10. Anani A, Visintin A, Petrov K, Srinivasant S. Alloys for hydrogen storage in nickel/hydrogen and nickel/metal hydride batteries. J. Pow. Sour. 1994; 47(3):261-275.doi:10.1016/0378-7753(94)87005-5.
11. Joubert JM, LatrocheM, PercheronGuegan A. Metallic-hydrides II:materials for electrochemical storage.MRS Bulletin. 2002; 27(9):694-698.
12. Akiba E, Okada M. Metallic hydrides III: body-centered-cubic solid solution alloys.MRS Bulletin. 2002; 27(9):699-703.
13. Viano RM, Stroud PC, Gibbons AF, McDowell MS,Conradi KF,Kelton KF.Hydrogenation of titanium-based quasicrystals.Phys Rev B Condens Matter. 1995;51(17):12026-12029.
14. Eliaz N, Eliezer D, Abramov E, Zander D, Köster U. Hydrogen evolution from Zr-based amorphous and quasicrystalline alloys.J. Alloys Compd. 2000; 305(1-2):272-281.doi:10.1016/S0925-8388(00)00717-9.
15. Sandrock G, Thomas G. Compilation of IEA/DOE/SNL hydride databases. IEA Technical Report. 1977.
16. James B Friauf. The crystal structure of two intermetallic compounds.J. Am. Chem. Soc. 1927;49(12):3107–3114.doi: 10.1021/ja01411a017.
17. James B Friauf. The Crystal Structure of Magnesium Di-Zincide. Phys. Rev. 1927;29:34–40. doi: http://dx.doi.org/10.1103/PhysRev.29.34.
18. Stein F, Palm M, Sauth G. Structure and stability of Laves phases. Part I. Critical assessment of factors controlling Laves phase stability.Intermetallics. 2004; 12(7-9):713–720. doi:10.1016/j.intermet.2004.02.010.
19. Sauthoff G.Intermetallics. 1995; VCH, Weinheim, Germany.
20. Livingston JD. Laves-Phase Superalloys? Phys. Stat. Sol. (a). 1992; 131(2):415–423. doi:10.1002/pssa.2211310215.
21. Anani A, Visintin A, Petrov K, Srinivasan S, Reilly JJ, Johnson JR, et al. Alloys for hydrogen storage in nickel/hydrogen and nickel/metal hydride batteries. J. Pow. Sour. 1994; 47(3):261-275. doi:10.1016/0378-7753(94)87005-5.
22. Shaltiel D, Jacob I, Davidov D. Hydrogen absorption and desorption properties of AB_2 Laves phase pseudobinary compounds. J. Less-Common Met. 1977;53(1):117-131. doi:10.1016/0022-5088(77)90162-X.
23. van Essen RM, Buschow KHJ. Composition and hydrogen absorption of C14 type Zr-Mn compounds.Mater. Res. Bull. 1980;15(8):1149-1155. doi:10.1016/0025-5408(80)90079-3.
24. Nishimiya N.Hydriding behaviors and equilibrium properties of Zr-Mn binary alloys.Mater. Res. Bull.1986;21(9):1025-1037. doi:10.1016/0025-5408(86)90217-5.
25. Roy L Johnston, Roald Hoffmann.Structure-Bonding Relationships in the Laves Phases.J.In. Gen. Chem. 1992; 616(10):105-120. doi:10.1002/zaac.19926161017.
26. David P. Shoemaker, Clara Brink Shoemaker.Concerning atomic sites and capacities for hydrogen absorption in the AB_2Friauf-Laves phases.J. Less-Common. Met. 1979;68(1):43-58. doi:10.1016/0022-5088(79)90271-6.
27. Dong-Myung Kim, Seok-WonJeon, Jai-Young Lee.A study of the development of a high capacity and high performance Zr–Ti–Mn–V–Ni hydrogen storage alloy for Ni–MH rechargeable batteries.J. Alloys Compd. 1998; 279(2):209-214. doi:10.1016/S0925-8388(98)00508-8.
28. Shaltiel D, Jacob I, Davidov D.Hydrogen absorption and desorption properties of AB_2 laves-phase pseudobinary compounds.J. Less-Common Met. 1977; 53(1):117-131.doi:10.1016/0022-5088(77)90162-X.
29. Klein B, Simon N, Klyamkine S, Latroche M, Percheron-Guegan A. Improvement of the thermodynamical and electrochemical properties of multicomponent Laves phase hydrides by thermal annealing. J. Alloys Compd. 1998; 280(1-2):284-289.doi:10.1016/S0925-8388(98)00702-6.
30. Visintin A, Peretti HA, Tori CA, Triaca WE.Hydrogen absorption characteristics and electrochemical properties of Ti substituted Zr-based AB_2 alloys.Int. J. Hydrogen Energy. 2001; 26(7):683-689. doi:10.1016/S0360-3199(00)00132-4.
31. Guo X, Wu E. Thermodynamics of hydrogenation for $Ti_{1-x}Zr_xMnCr$ Laves phase alloys.J.AlloysCompd. 2008;455(1-2):191-196. doi:10.1016/j.jallcom.2007.01.066.
32. Rietveld HM.A Profile Refinement Method for Nuclear and Magnetic Structures.J.Ap.Cryst. 1969; 2:65 – 71. doi:10.1107/S0021889869006558.
33. Makridis SS, Ioannidou A, Zupanic E, Prodan A, Kikkinides ES, Stubos AK. Effect of V substitution on the composite Zr-Ti-Cr-V-Ni intermetallic hydride. Proceed. Mat. Sc. Forum. 2010; 636-637:887-894.doi: 10.4028/www.scientific.net/MSF.636-637.887.
34. Soubeyroux JL, Bououdina M, Fruchart D, Pontonnier L. Phase stability and neutron diffraction studies of Laves phases $Zr(Cr_{1-x}M_x)_2$ with M=Mn, Fe, Co, Ni, Cu and 0<x<0.2 and their hydrides. J. Alloys Compd. 1995; 219:48-54.
35. Bououdina M, Menier P, Soubeyroux JL,Fruchart D.Study of the system $Zr_{1-x}Ti_x(Cr_{0.5}M_{0.4}V_{0.1})_2 - H_2$ ($0 \leq x \leq 0.2$, M=Fe, Co, Ni).J.Alloys Compd.1997; 253-254:302-307.doi:10.1016/S0925-8388(96)02901-5.
36. Ioannidou A, Makridis SS, Zupanic E, Prodan A, Kikkinides ES, Stubos AK. Structural and hydrogenation properties of $Zr_{0.9}Ti_{0.1}Cr_{1.2-x}V_{0.8}Ni_x$ (x=0, 0.4) compounds.Proceed. Mat. Sc. Forum. 2010; 636-637:880-896. doi: 10.4028/www.scientific.net/MSF.636-637.880.